

Using Remote Sensing Techniques and Field-Based Structural Analysis to Explore New Gold and Associated Mineral Sites Around Al-Hajar Mine, Asir Terrane, Arabian Shield

Abdullah R. Sonbul^(a), Mohamed. K. El-Shafei^(a,b), Adel Z. Bishta^(a,c)

^(a)Faculty of Earth Sciences, King Abdulaziz University

^(b)Geology Department, Faculty of Science, Suez Canal University, Ismailia, Egypt

^(c)Nuclear Materials Authority, Cairo, Egypt

mshafei@kau.edu.sa

Abstract: Modern earth resource satellites provide huge amounts of digital imagery at different resolutions. These types of data are considered to be one of the most significant sources of data for mineral exploration. Image processing techniques were applied to the exposed rocks around the Al-Aqiq area of the Asir terrane in the southern part of the Arabian Shield. The area under study has two sub-parallel N-S trending metamorphic belts. The first belt is located southeast of Al-Aqiq, where the Al-Hajar Gold Mine is situated. It is essentially composed of metavolcanics and metasedimentary rocks, and it is emplaced by different plutonic intrusions of primarily diorite, syenite and porphyry granite. The second belt is located northwest of Al-Aqiq, and it is composed of metavolcanics and metasedimentary rocks and is emplaced by granite bodies. The current study aims to detect the alteration zones around the Al-Hajar gold prospect. Digital satellite imageries, including Landsat ETM+ Multispectral and panchromatic (30 and 15 m resolution) and SPOT-5 Multispectral and panchromatic (10 and 5 m resolution), are used to distinguish the alteration zones. Areas with similar spectral signatures to the prospect area in the nearby metamorphic belt are considered target areas for field verification. The relationships between the alteration zones, the mineral deposits and the structural elements are used to visualize the ore-bearing alteration zones in the subsurface. Structurally, the prospect area is highly sheared and shows different types of alterations. The alterations that are associated with shear zones are promising targets for mineral exploration. The target area displays dextral-ductile shearing top-to-the-north and a deformed mineralized quartz vein-system in the metasedimentary units. The metamorphic rocks are overprinted by an alternating isoclinal series of subvertical axial plane anticline and syncline folds. Local thrust planes and imbrications are detected along the contacts between the plutonic intrusions and the metamorphic units. The host rocks of mineralization are green-schist facies metasedimentary and metavolcanic rocks of pre-Cambrian age. Two types of mineralization are determined. The first are the porphyry-type ore deposits around the Al-Hajar open-pit gold mine, and the second are vein-type ore deposits in the target area. Both of the two areas are promising for subsurface mining.

[Abdullah R. Sonbul, Mohamed. K. El-Shafei, Adel Z. Bishta. **Using Remote Sensing Techniques and Field-Based Structural Analysis to Explore New Gold and Associated Mineral Sites Around Al-Hajar Mine, Asir Terrane, Arabian Shield.** *Researcher* 2015;7(9):19-35]. (ISSN: 1553-9865). <http://www.sciencepub.net/researcher>. 3

Keywords: Image processing, alteration zones, shear zone, Arabian Shield, Al-Aqiq area, Al-Hajar gold prospect, porphyry-type deposits.

1. Introduction

The study area is located between latitudes 19° 50', 20° 30' N and longitudes 41° 25', 42° 25' E (Fig. 1). It is located in the northwestern portion of the Asir terrane approximately 80 km southeast of Al-Aqiq City. The study area is composed essentially of metasediments and metavolcanics. Numerous intrusive igneous bodies of Precambrian age also dominate the study area and the Arabian Shield, (AS). The AS comprises five major tectonic terranes: Asir, Al Hijaz, Madyan, Afif, and Ar Rayn. The first three terranes are formed of an intraoceanic island arc, and they are located at the western part of the Shield. The other two are of continental origin and are located on the eastern part of the Shield. These tectonic terranes are separated by four suture zones that are decorated

by ophiolite belts. The sutures include: Bir Umq, Yanbu, Nabitah, and Al-Amar (Al-Shanti, 2009). A recent geological study on the dioritic igneous body of the Mount Ablah mining prospect to the west of the study area was conducted by Bamoussa (2013).

Generally, the area under study has not been previously subjected to detailed geological studies. Reconnaissance geological mapping of the study area was conducted within the regional map of the Al Aqiq Quadrangle on the scale of 1:100,000 by Greenwood in 1975.

The current work is a field-based study that uses digital image processing techniques to detect alteration zones. The alteration zones are good field criteria for mineralization (e.g., Deksis and Koeberl,

2004; El-Shafei, 2011; Doyle et al., 2013; Kolb et al., 2004).

The spectral signature of the Al-Hajar gold mining prospect is used in this study as a key to locate new similar sites as target areas in the surrounding metamorphic belt. The results of the current study may be used as an applicable model for any other low-grade metamorphic belts in the AS where alteration zones are dominant.

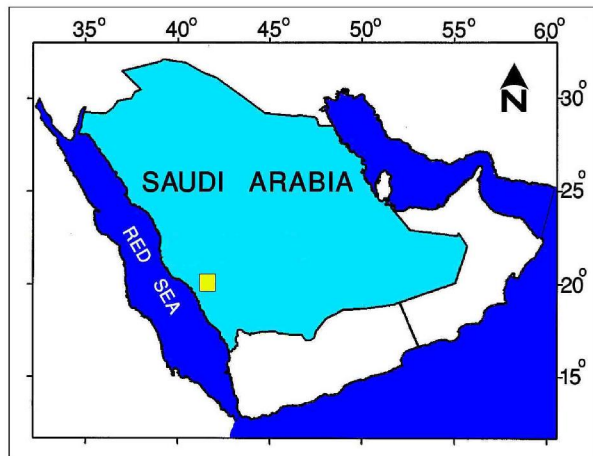


Figure 1. Location map of the study area

Image processing techniques for the remote sensing data have been used for mineral exploration, geological interpretation and mapping by many authors (e.g., Abrams, et al., 1983; Davis and Berlin, 1989; Davis and Berlin, 1989; Sultan et al., 1986; Gibson and Power, 2000; Madany and Bishta, 2002; Gupta, 2003; Jutz, and Chorowicz, 1993; Lillesand et al., 2004; Wielen et al., 2004; Kavak and Cetin, 2007; Bishta, 2008; Amer et al., 2009; Bishta, 2010; Sabins, 1999; El Janati et al., 2013; Guha et al., 2014). Antonielli et al., (2009) used remote sensing optical images that were integrated with ancillary data and ground truth information for the detailed mapping of the volcano-sedimentary succession of the Lower Dogali Formation in NE Aritrea. Haselwimmer et al. (2010) classified granitoid intrusive rocks and altered rhyolitic volcanic rocks of eastern Adellaide Island using the spectral properties of the ASTER data.

2. Methodology

The first phase of the current study is remote sensing analysis. It is used to discriminate the different lithologic units, trace the major structural lineaments and detect the alteration zones. The second phase includes the field verification and collection of the available structural measurements for the geometrical analysis.

Two main types of digital satellite imageries are used: Landsat-7 Enhanced Thematic Mapper plus

(ETM+) data, and SPOT-5 data. The remotely sensed raw data of the study area are included in the Landsat-7 data with a scene number of path/raw = 175/40, and in the SPOT-5 data, the scene number is path/raw = 139/310. The visible, near-infrared and short wave infrared bands of the Enhanced Thematic Mapper ETM+ data are also processed.

The Landsat ETM+ data consist of 7 bands. The infrared ETM+ bands were characterized by the wavelength intervals of 760 to 900 nm (band 4), 1500 to 1750 nm (band 5) and 2080 to 2350 nm (band 7). The visible ETM+ bands, 1, 2 and 3, were characterized by wavelength intervals of 450 to 520 nm for band 1, 520 to 600 nm for band 2 and 630 to 690 nm for band 3. The Landsat ETM+ imagery data were characterized by a spatial resolution of 30 m (multispectral bands 1, 2, 3, 4, 5 & 7), 60 m (thermal band 6) and 15 m (panchromatic band 8).

The visible ETM+ bands are used to determine the most reliable identifications of the different rock units, while panchromatic band 8 is very useful for visual structural and lithological interpretation. The supplementary data that covers the study area includes geological maps of the previous work and the topographic maps on a scale of 1:50,000. The topographic maps were used in the processing of the geometric corrections of the Landsat ETM+ and SPOT-5 data.

The SPOT-5 data comprises 5 bands; the visible bands are characterized by wavelength intervals of 500 to 590 nm (band 1) and 610 to 680 nm (band 2) and near infrared bands from 780 to 890 nm (band 3). The short wave infrared band has wavelength intervals of 1580 to 1750 nm (band 4). The panchromatic band was characterized by wavelength intervals of 480 to 710 nm (band 5). The satellite imagery of the SPOT-5 data is characterized by a spatial resolution of 10 m (multispectral bands 1, 2, 3), 20 m (SWIR band 4) and 2.5 m (panchromatic band 5).

The main steps of image processing and interpretation for both the Landsat ETM+ and SPOT-5 data of the study area were conducted using the following methods:

- 1- Rectification and image enhancement of the Landsat ETM+ and SPOT-5 data,
- 2- Regional geological mapping using the Landsat ETM+ data,
- 3- Image ratios using the Landsat ETM+ data and isolating the alteration zones, and
- 4- Detailed geological mapping of the prospect and target areas using the SPOT-5 data.

2.1 Rectification of the SPOT-5 and the Landsat ETM+ data and image enhancement

Raw digital satellite data usually includes geometric distortions due to the sensor geometry, the scanner, platform instabilities, the earth rotation, the

earth curvature, etc., and it is necessary to correct for and adapt these distortions (Mather, 1987; Lillesand et al., 2004; Richards, 1995). The geometric correction is conducted for the digital data of the ETM+ bands of

the study area using two main steps for image rectifications: rectification of a panchromatic ETM+ band 8 and rectification of the multispectral ETM+ bands (1 to 7).

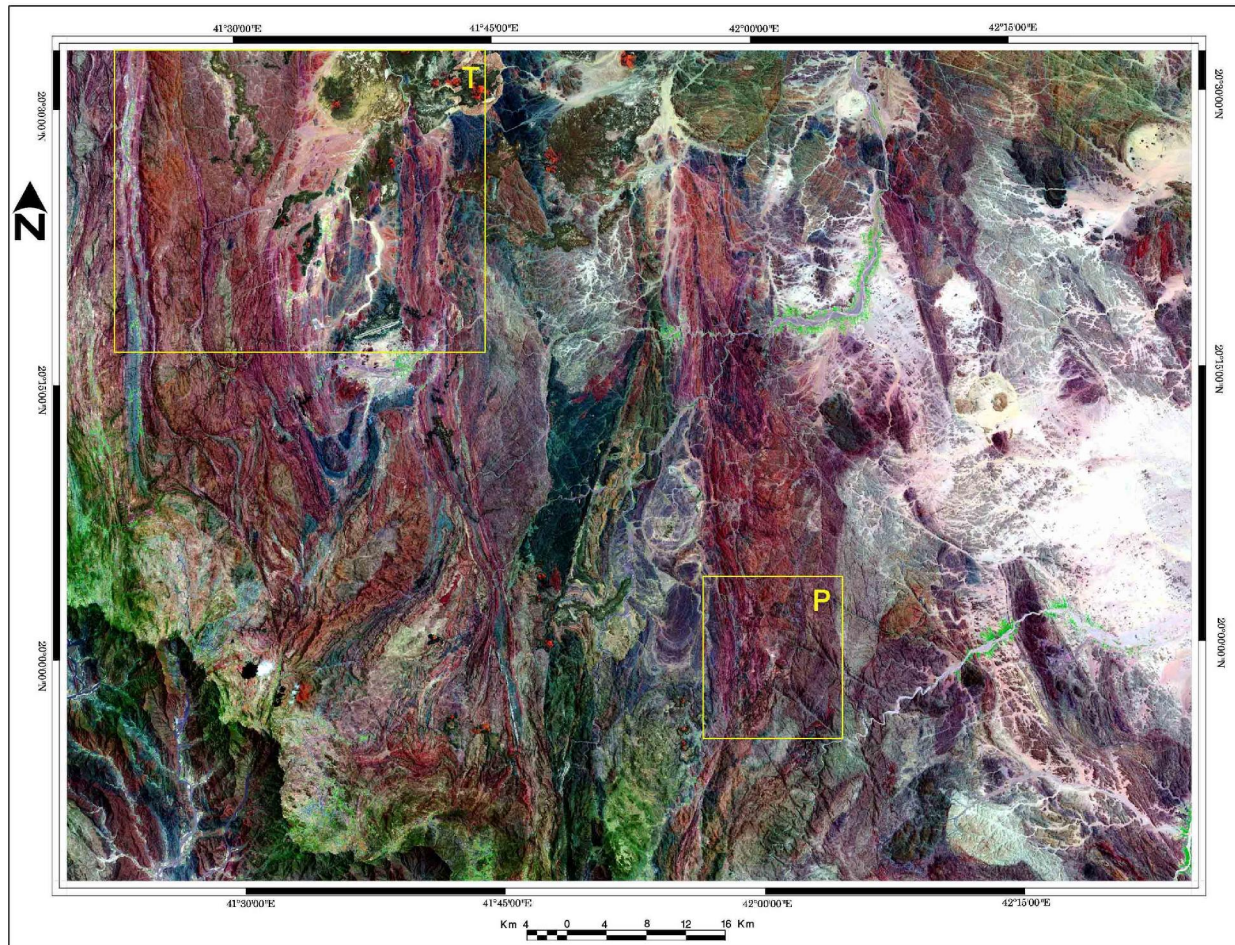


Figure 2. False color composite Landsat image of the study area, ETM+ bands 7, 4, 2 in RGB, showing the prospect area (P; Al-Hajar mine) and the target area (T; newly detected area). (Original scale 1:100,000).

The correction in the first step occurred by collecting 185 well-distributed ground control points that were selected from the topographic sheets (scale 1:50,000) for the investigated area using the image to map method. The overall accuracy of the transformation is indicated by averaging the errors in the reference points and the root mean square error (RMS = 0.63, Bernstein, 1978). The cubic interpolation method is used in the resampling processing. The rectified panchromatic ETM+ band is then used as a geo-referenced base for the correction of the 6-multispectral ETM+ bands (1 to 7). In the second step, we used the image-to-image method. The geometric corrections of the SPOT-5 data were performed using the same methods.

The image enhancement procedure includes the production of a raw image that is more interpretable for a particular application (PCI Geomatica, 2003).

The histogram equalization enhancement technique was applied to the ETM+ data from the study area to increase the contrast of the images (Schowengerdt 1983; Mather 1987; Lechi 1988). The enhanced false color composite Landsat ETM+ image (Fig. 2) for the study area was constructed from bands 7, 4 and 2, shown in red, green and blue, respectively, on a scale of 1:100,000. This image is used as a base map to construct the regional geological map of the investigated areas.

The SPOT-5 digital data are used to construct large scale 1:20,000 images for both the prospect area of the Al-Hajar gold mine and the target area in the region to the north and northwest of the Al-Aqiq airport. The enhanced false color composite SPOT image for the prospect area (Fig. 3) is a result of bands 4, 3 and 1, shown in red, green and blue, respectively, with an original scale of 1:20,000. The enhanced false

color composite SPOT image for the target area (Fig. 4) is constructed from bands 4, 3 and 1, shown in red, green and blue, respectively, with an original scale of

1:20,000. These two SPOT images are used as the base maps for tracing and constructing the detailed geological maps of the prospect and target areas.

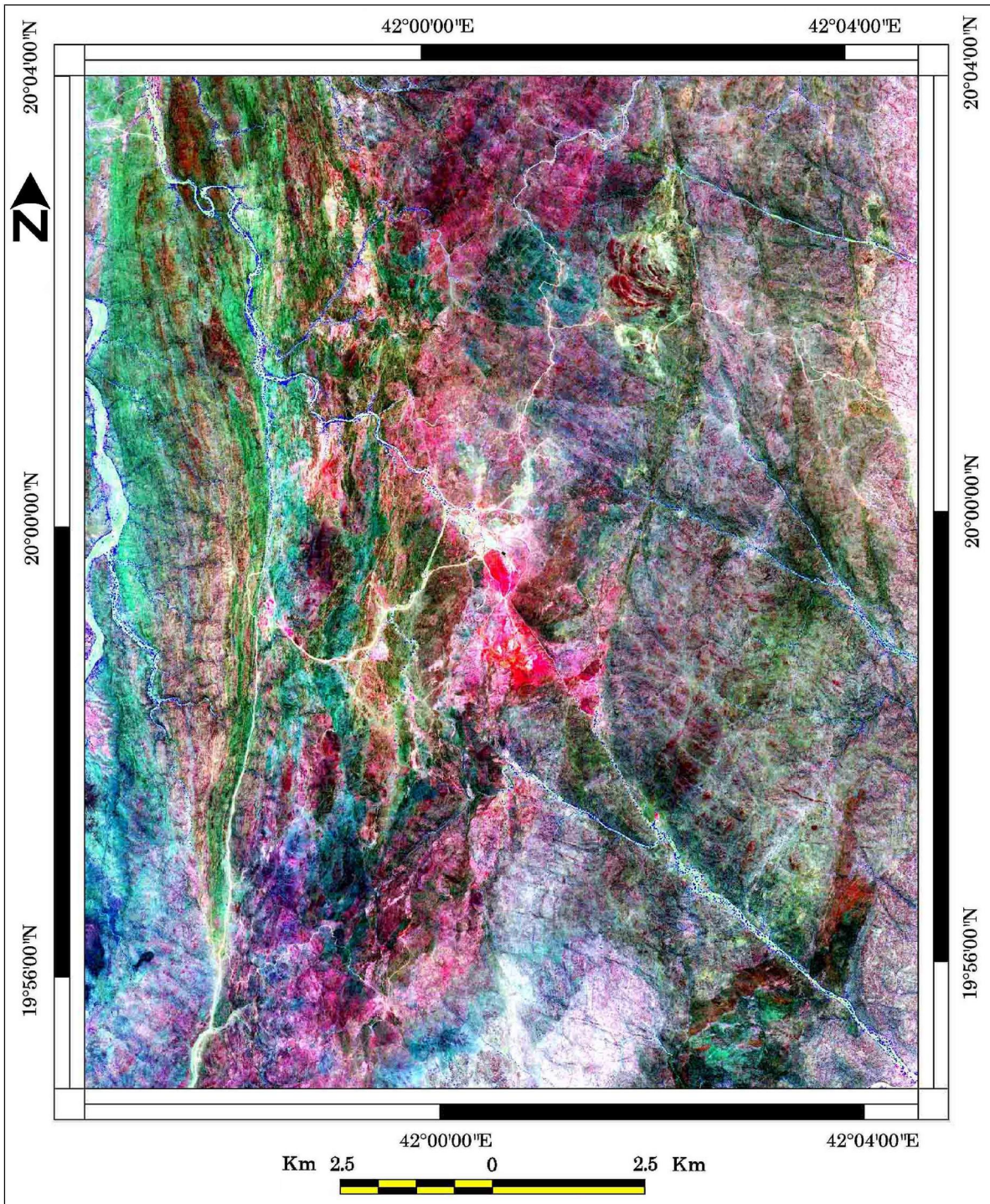


Figure 3. False color composite SPOT image of the prospect area (Al-Hajar mine; the reddish zone), bands 4, 3, 1 in RGB. (Original scale 1:20,000).

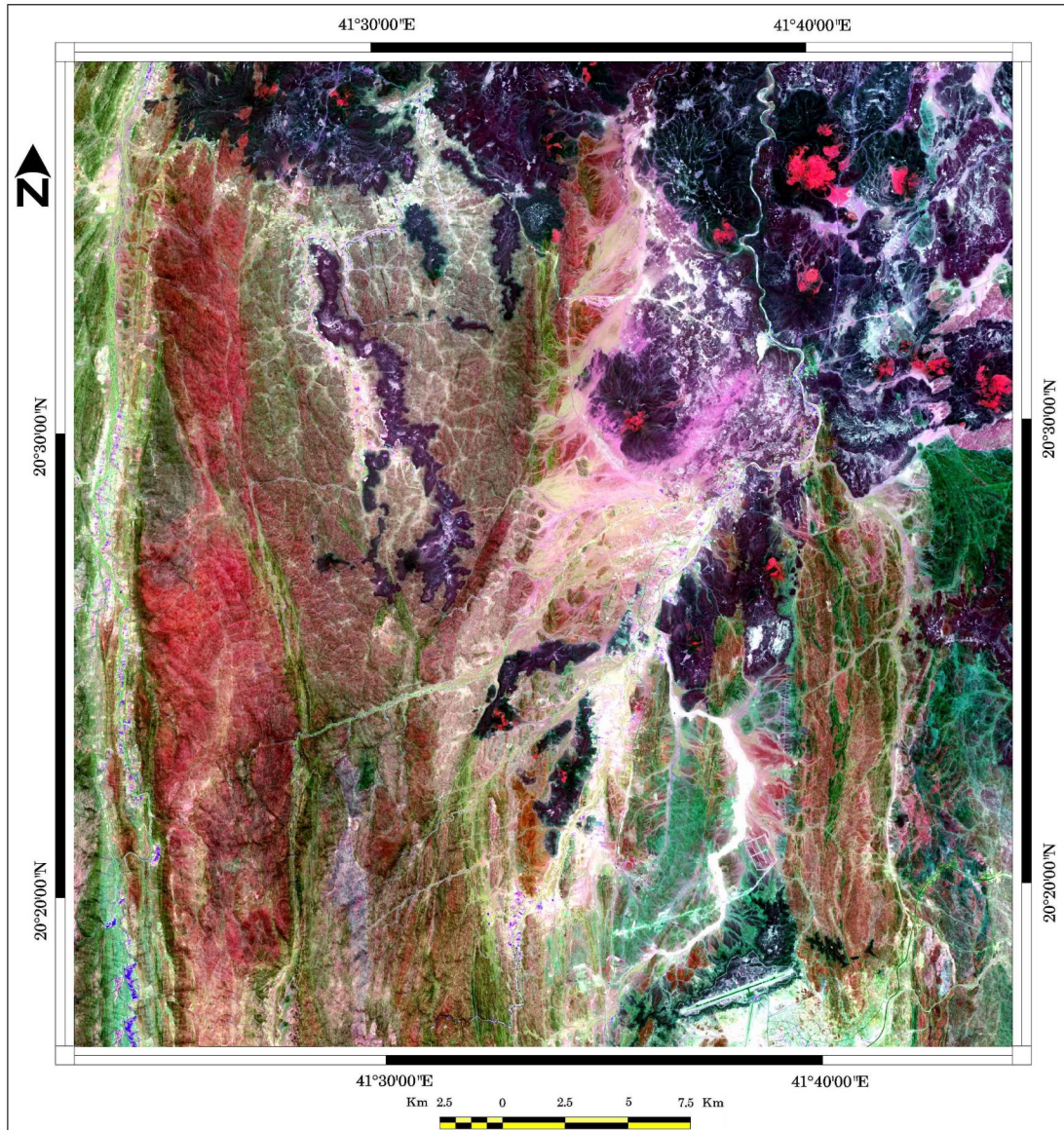


Figure 4. False color composite SPOT image of the target area (North & Northwest of El-Baha airport), bands 4, 3, 1 in RGB. (Original scale 1:20,000).

2.2 Regional geologic setting of the Al-Aqiq area

The area around Al-Aqiq in the southern Asir terrain of the Arabian Shield is characterized by a complex tectonic setting and a diversity of rock units. In this study, a simplified regional geologic map (Fig. 5) on the scale of 1:100,000 is constructed based on the interpretation of the false color composite Landsat image of the study area (Fig. 2) and field verification. The main rock units exposed in the mapped area belong to the Precambrian age and include metamorphic tectonites that are intruded by different plutonites. A volcano sedimentary succession of the Ablah group is exposed in the middle of the mapped area. Younger pyroclastic rocks and basaltic flows

were also recorded. The plutonic rocks predominately comprise diorite, gabbro, porphyritic granite and syenite. The metamorphic rocks trend primarily north-to-south and comprise low-grade greenschist facies rocks with steeply east and west dipping foliations.

The presence of shearing was the most significant tectonic element recorded within the entire rock of the mapped area (Fig. 5). Shearing that is almost north-to-south is clearly developed along the boundary between the metamorphic rocks and the intruded plutonic bodies. This is characterized by a dextral sense of shear, and it developed between the geologic contacts of the different metamorphic units. Shear-sense criteria were also recorded in the syn-

tectonic igneous bodies that intruded the metamorphic

units.

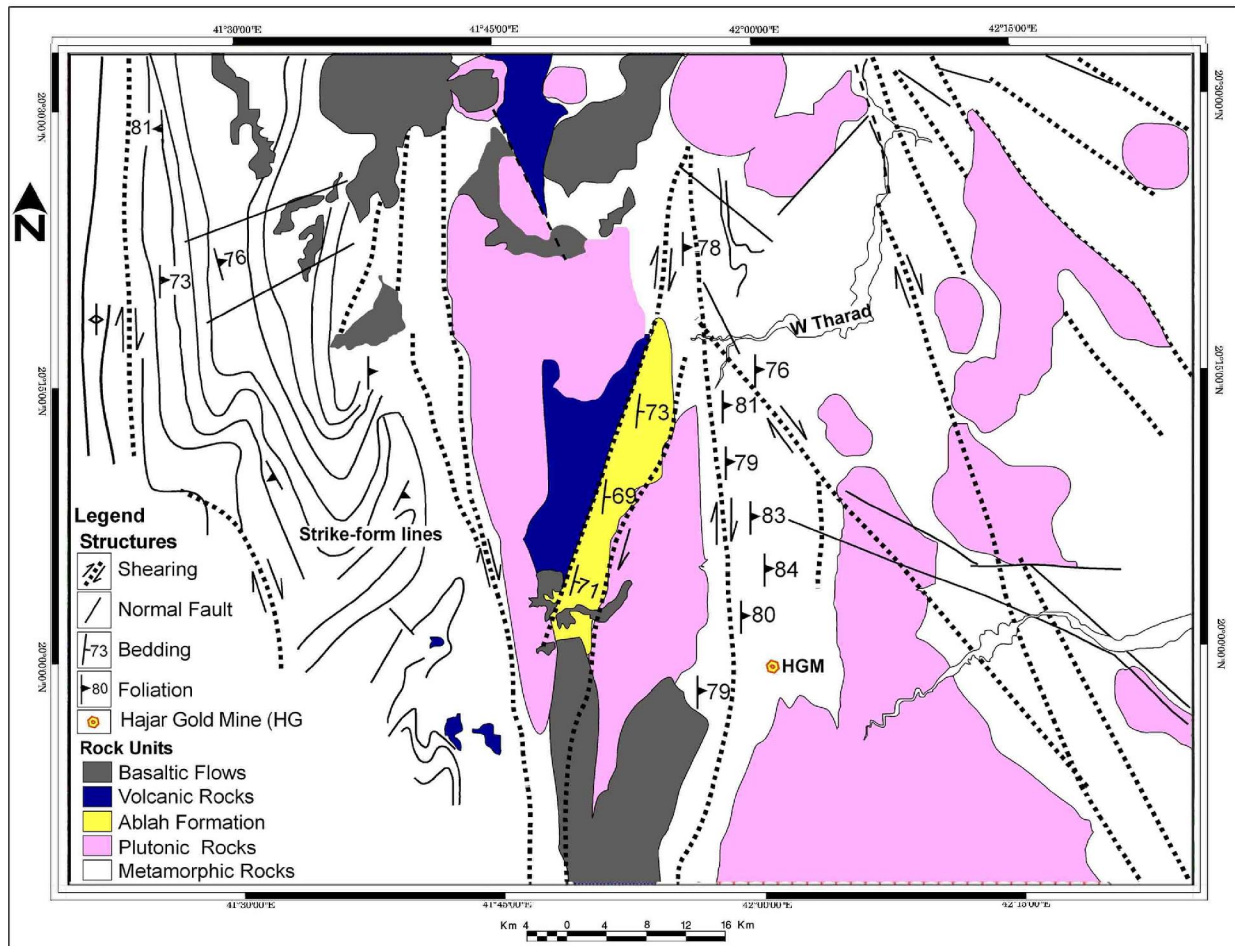


Figure 5. Regional geological map of the study area. The false color composite Landsat image of Fig. 2 is used as a base map to trace the geologic boundaries. (Original scale 1:100,000).

2.3 Image ratios of the Landsat ETM+ data

The addition, subtraction, multiplication and division of the pixel brightness from two bands of the image data to form a new image are particularly simple transformations to apply and can often be implemented in hardware using a look-up table (Richards 1995). The band-ratio technique is applied by dividing the digital number (DN) pixel values of one band with the DN pixel values of another band. Bishta (2004) used the Landsat ETM+ band ratios for the lithologic discrimination of the Gabal Qattar area in the Eastern Desert of Egypt.

The spectral band ratio is one of the most common and powerful techniques applied for mapping the minerals of alteration zones (clay, alunite and iron minerals) (Sabins 1999). The recognition of hydrothermal altered rocks that are associated with mineral deposits, such as gold, was performed using image processing techniques, such as band-ratio images and color ratio composite images. The spectral

bands of ETM+ are well-suited for recognizing the assemblage of altered minerals. The hydrothermal minerals that were detected by the Landsat image processing of the data of PA and the selected TA can be classified into two groups: 1) hydroxyl (clay minerals) and hydrated minerals (alunite and jarosite) that are detected by a band ratio of 5/7; and 2) minerals containing iron (hematite and goethite,) that are detected by a band ratio of 3/1. By applying these techniques, we recognized zones of altered rocks within the target area.

2.3.1 Alteration zones of the prospect area

The image ratios of the Landsat ETM+ bands, 3/1 and 5/7, are constructed for the prospect area, as shown in Figs. 6 & 7, respectively. The ratio of the Landsat band, 3/1, (Fig. 6) is used mainly to detect the iron oxide alteration zones. The ratio appears as a bright gray signature tone over the metavolcanic rocks, which suggests a high 3/1 DN value.



Figure 6. Image ratio of the Landsat ETM+ band 3/1 for the prospect area. The iron oxide alteration zones are in bright gray.

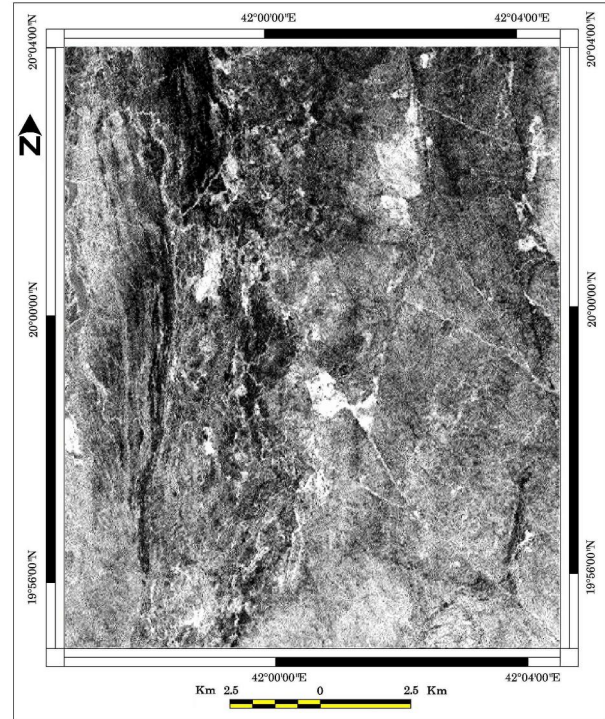


Figure 7. Image ratio of the Landsat ETM+ band 5/7 for the prospect area. The clay mineral alteration zones in bright gray.

Therefore, they are iron-stained hydrothermally altered rocks. The image ratio of the Landsat band, 5/7 (Fig. 7), was used for the prospect area to measure the intensity of the hydroxyl absorption in the 2.2 to 2.4 μm region. This ratio is applied because band 5 does not fall within the confines of the Fe-aluminosilicate-related or hydroxyl-related absorption features; however, band 7 is within the hydroxyl absorption wavelength (Sultan et al., 1987). The 5/7 band-ratio image (Fig. 7) shows a light tone signature that characterizes the alteration zones of clay minerals in the prospect area due to the low content of hydroxyl-bearing minerals and opaques.

A traced map of the alteration zones of iron oxides are shown in Figure 8, and the clay minerals are shown in Fig. 9. Both are interpreted from the image ratios of the Landsat ETM+ bands (Fig. 6 and Fig. 7), respectively. The alteration zones of the prospect area are associated with the previously revealed mineralized gold areas over the metavolcanic rocks. The same image processing is applied for the target area to detect the alteration zones that are associated with potential gold-mineralized rocks.



Figure 8. Alteration zones of the iron oxides interpreted from the image ratio of the Landsat ETM+ band 3/1 in Fig. 6 for the prospect area.

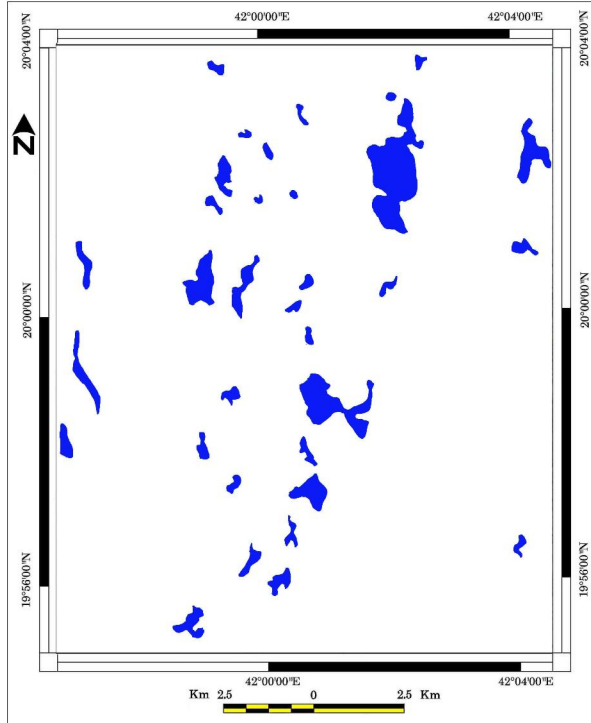


Figure 9. Alteration zones of the clay minerals interpreted from the image ratio of the Landsat ETM+ band 5/7 in Fig. 7 for the prospect area.

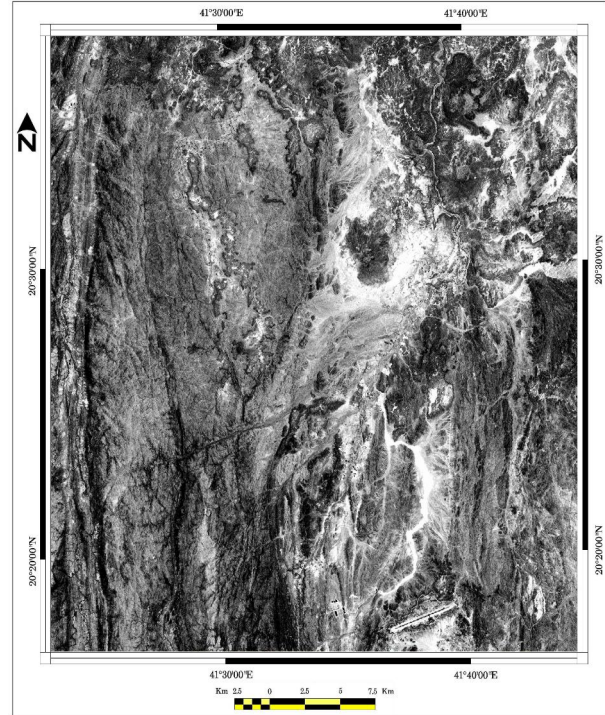


Figure 10. Image ratio of the Landsat ETM+ band 3/1 for the target area. The iron oxide alteration zones are in bright gray.

2.3.2 Alteration zones of the target area

The image ratios of the Landsat ETM+ bands, 3/1 and 5/7, are applied for the target area (T), as shown in Fig. (10) and Fig. (11), respectively. The ratio of Landsat band, 3/1, (Fig. 10) is used primarily to detect the iron oxide alteration zones in the target area. It shows a bright gray signature tone over the metamorphosed sedimentary (metasediments) rocks and some metavolcanic rocks, suggesting a high 3/1 DN value. Thus, they were determined to be iron-stained hydrothermally altered rocks.

The image ratio of the Landsat ETM+ band, 5/7, (Fig. 11) is used as a measure of the intensity of the hydroxyl absorption in the 2.2 to 2.4 μm region. The Landsat 5/7 band-ratio image of the target area (Fig. 11) exhibits a light tone signature that characterizes the alteration zones of the clay minerals. Light tone refers to the low content of hydroxyl-bearing minerals and opaques.

Figure 12 and Figure 13 show traced maps of the alteration zones of both iron oxides and clay minerals, respectively, as interpreted from the image ratios of the Landsat ETM+ bands (Figs. 10 & 11) for the target area. The most altered zones of the target area are restricted to metasedimentary and some metavolcanic rocks.

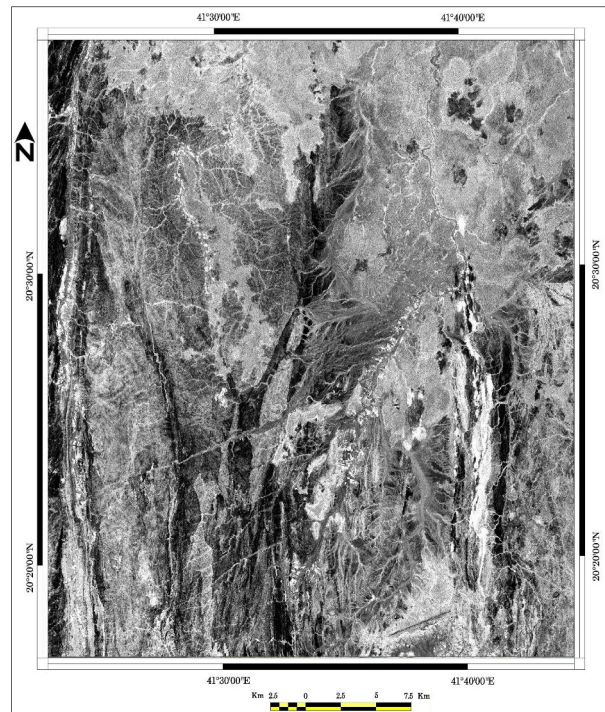


Figure 11. Image ratio of the Landsat ETM+ band 5/7 for the target area. The clay mineral alteration zones are in bright gray.

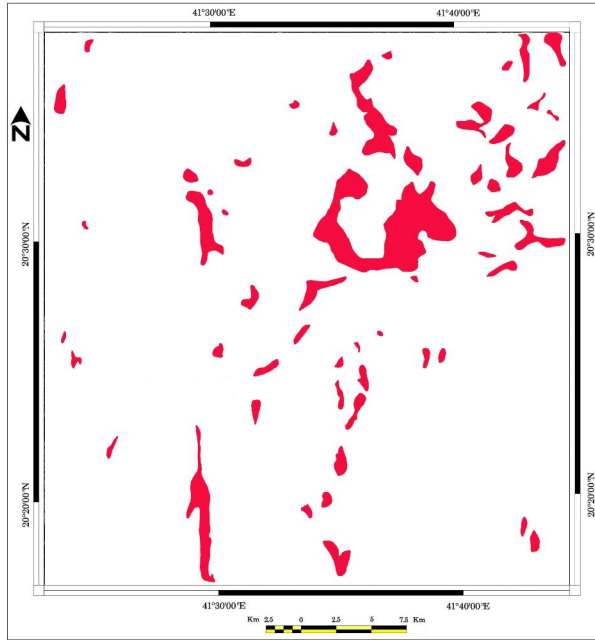


Figure 12. Alteration zones of the iron oxides interpreted from the image ratio of the Landsat ETM+ band 3/1 in Fig. 10 for the target area.

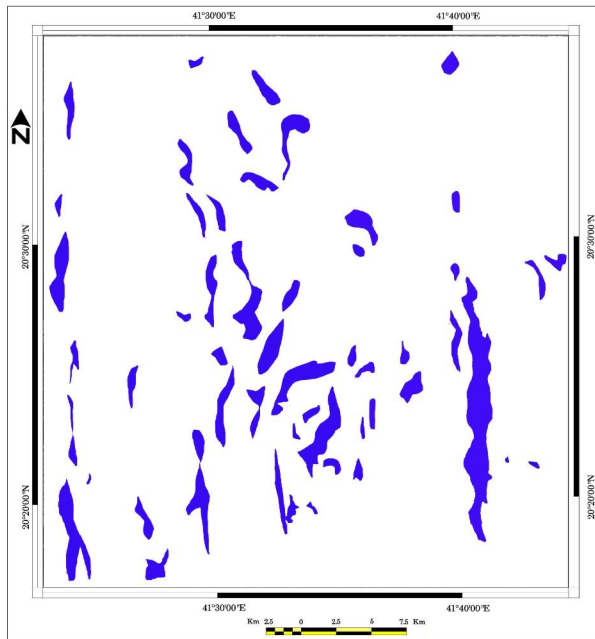


Figure 13. Alteration zones of the clay minerals based on the image ratio of the Landsat ETM+ band 5/7 in Fig. 11 for the target area. Note the N-S orientation of the traced zones.

3. Geologic and structural setting of the prospect and target areas

Two areas within two subparallel metamorphic belts were carefully investigated during this study. The first area is the prospect area, “P,” of the Al-Hajar

Gold Mine. It is located in the metamorphic belt to the east of Al-Aqiq (Fig. 2). The second area is situated northwest of Al-Aqiq and is called target area “T”, based on the image processing analysis. Intensive field work is conducted to delineate and investigate the role of the structural elements in controlling the distribution of the alteration zones and the mineral occurrence. We also performed geometrical analysis to build a 3D geometry of the ore deposits. The target area is a new promising area of mineral occurrences that is similar to the area of the Al-Hajar mine prospect.

A detailed geological map of the prospect area is shown in Figure (14). The false color composite SPOT image (Fig. 3) was used as a base map from which the geologic contacts and the major lineaments were traced. It was constructed from an original scale of 1:20,000. The mapped units and the structural elements were verified in the field to determine their relationship in controlling the alterations and the mineralization.

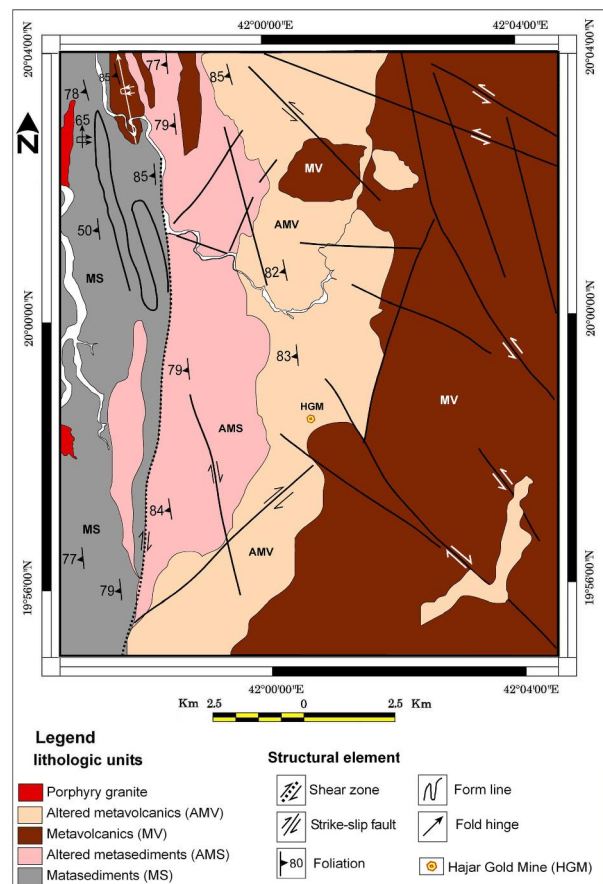


Figure 14. Detailed geological map of the prospect area. The false color composite SPOT image of Fig. 3 is used as a base map to trace the geologic boundaries. (Original scale 1:20,000).

The detailed geological map of the target area (T) in the original scale of 1:20,000 (Fig. 15) was traced from the false color composite SPOT image in Figure (4). It was verified in the field to determine the main lithological rock units and the structural elements that controlled the alteration zones in the target area (T).

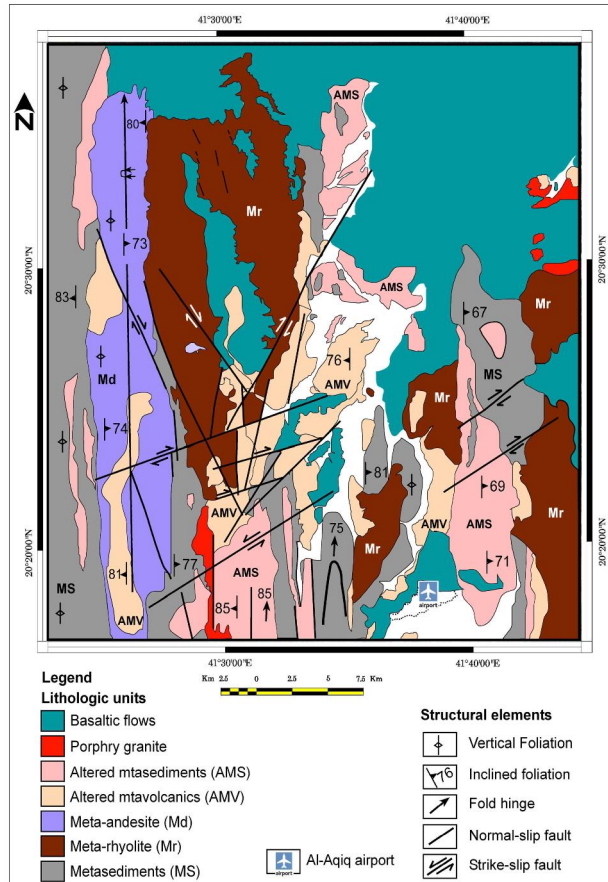


Figure 15. Detailed geological map of the target area. The false color composite SPOT image of Fig. 4 is used as a base map to trace the geologic boundaries. (Original scale 1:20,000).

The Al-Hajar area (Fig. 14) is a part of the north-south trending metamorphic belt located to the east of Al-Aqiq city. The belt is of low-grade greenschist and locally reaches amphibolite facies conditions. The main rock units are metasediments and metavolcanics. Slate, phyllite, metaconglomerate and schist are the metasediment units, while rhyolite, andesite and metatuffs are the main metavolcanic units (Fig. 14). The metasediments and metavolcanics show an intensive degree of shearing and the presence of alteration zones. Shearing is recorded either as a

plastic (Fig. 16a) or as a plastic-brittle deformation (Fig. 16b). The belt is simply a series of large-scale, nearly subvertical anticline and syncline folds. The meso-scale folds of a similar type (Fig. 16c) or the overturned folding (Fig. 16d) are also preserved. The field data and geometrical analysis indicate the presence of two fold generations (F_1 and F_2). F_1 -folds are a series of isoclinal anticline and syncline folds of gently plunging axis due north, where F_2 trends $N 10^\circ E$ and dips 65 degrees.

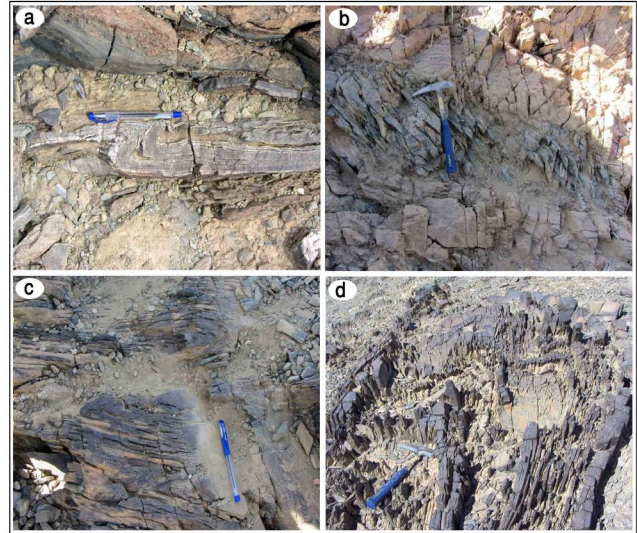


Figure 16. Field photographs of shear-sense indicators: (a) asymmetrical Z-shaped fold in phyllite showing the dextral-sense of the shear "top-to-the-north" in the target area, (b) deformed diorite shear-band in the alkali granite along the western contact in the metamorphic rocks of the prospect belt, (c) similar folds in phyllite, looking W, (d) plane view of the overturned north-trending anticline fold in phyllite; note the development of a pencil and rod structure; both plunge 65° due $N 10^\circ E$.

The development of imbricated thrust stacks are recorded in the metasediments (Fig. 17a) along the western contact with the plutonic rocks. The thrust movement is directed north. The folded and mineralized quartz veins (Fig. 17b) are commonly recognized within the target area. The presence of folded and boudinaged mineralized quartz veins throughout the investigated area are indicative of a polyphase deformation. They developed post- D_1 and overprinted by later deformational phases (D_2 and D_3).

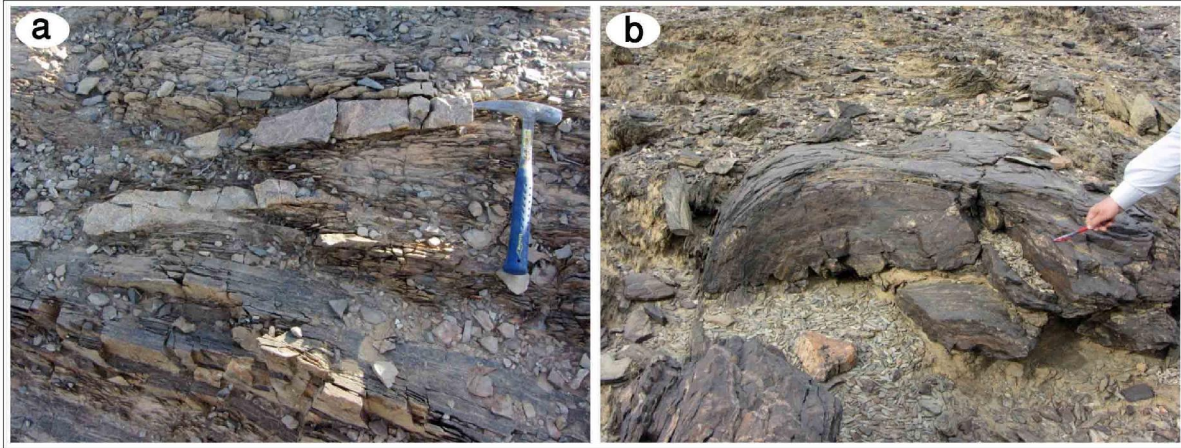


Figure 17. Field photographs showing the compressional-related structures: (a) The North-directed thrust movement and the development of imbricated thrust stacks along the western contact of the metamorphic belt with the plutonic intrusions and (b) the folded thick body of mineralized quartz in the target area.

3.1 Mineral (deposit) indicators

The collected field data during this study confirm the presence of both porphyry-type deposits and hydrothermal vein-type deposits in the studied metamorphic units. The evidence includes:

- Hydrothermal breccia (Fig. 18a), which is recorded in some locations as small and large bodies, particularly in the metavolcanic domain.

- Porphyritic granite that is exposed as a dike-like intrusion (Fig. 18b) within the metamorphic units. It is also overprinted by the shearing phase, which is clearly recognized along the contact with the metamorphic rocks.

- Dike-like bodies and thick veins of jasper (Fig. 18c), which run parallel to the foliation planes and developed in the metasediments.

- Alteration zones. Different alteration zones with varying degree of alterations are recorded in many outcrops throughout the entire belt. They are folded as an indication of their progress after folding. They are mostly shear-zone controlled (e.g., Blenkinsop, and Doyle, 2014).

- Iron gossans. The iron gossans include small and huge bodies.

- Mineralized quartz veins, which run parallel to the axial plane foliation and are folded and show boudinage structures (Fig. 18d). Subparallel veins of different thicknesses and similar attitudes that are preserved in the metasediments (Fig. 18e) northwest of Al-Aqiq are also recognized.

3.2 Hydrothermal alterations

Typically, the hydrothermal fluids find their way through the pre-existing fractures, and they carry

many metals in addition to silicates and other non-metallic materials (e.g., Gustafson and Quiroga, 1995; Williams-Jones and Heinrich, 2005). The mineral-rich fluids rise and dissolve other minerals on their path once the solution has cooled in the fracture of the rock-creating mineralized veins (e.g., Cox, 1999).

The alteration zones that are recognized in the investigated areas are considered to be epigenetic because they are primarily overprint regional metamorphic fabrics and they developed with and along the shear zones. Additionally, the mineralized quartz veins were deformed (folded and even boudinaged), and they developed parallel to the foliation planes. They possibly invaded the post- D_1 and pre- D_2 deformational phase and are associated with the regional metamorphism.

Outcrops of significant indications of mineralization are shown in Fig. (19). Most of the foliations are either subvertical (Fig. 19a) or have steeply dipping planes. In many outcrops, the alteration zones obliterate the nature and origin of the altered rock and appear light reddish in color (Fig. 19b) or pale yellow in color. Iron gossans of meso-scale size (Fig. 19c) or even mountain size (Fig. 19d) were found in many locations, specifically in the metasedimentary rocks. The mineralized quartz veins were overprinted by the later deformation phases and preserved as lenses (Fig. 19f) or isolated pockets in the area parallel to the metamorphic fabrics. The altered rocks were collected from the open pit site, and then the associated minerals were separated in the Al-Hajar mine prospect (Fig. 19f).

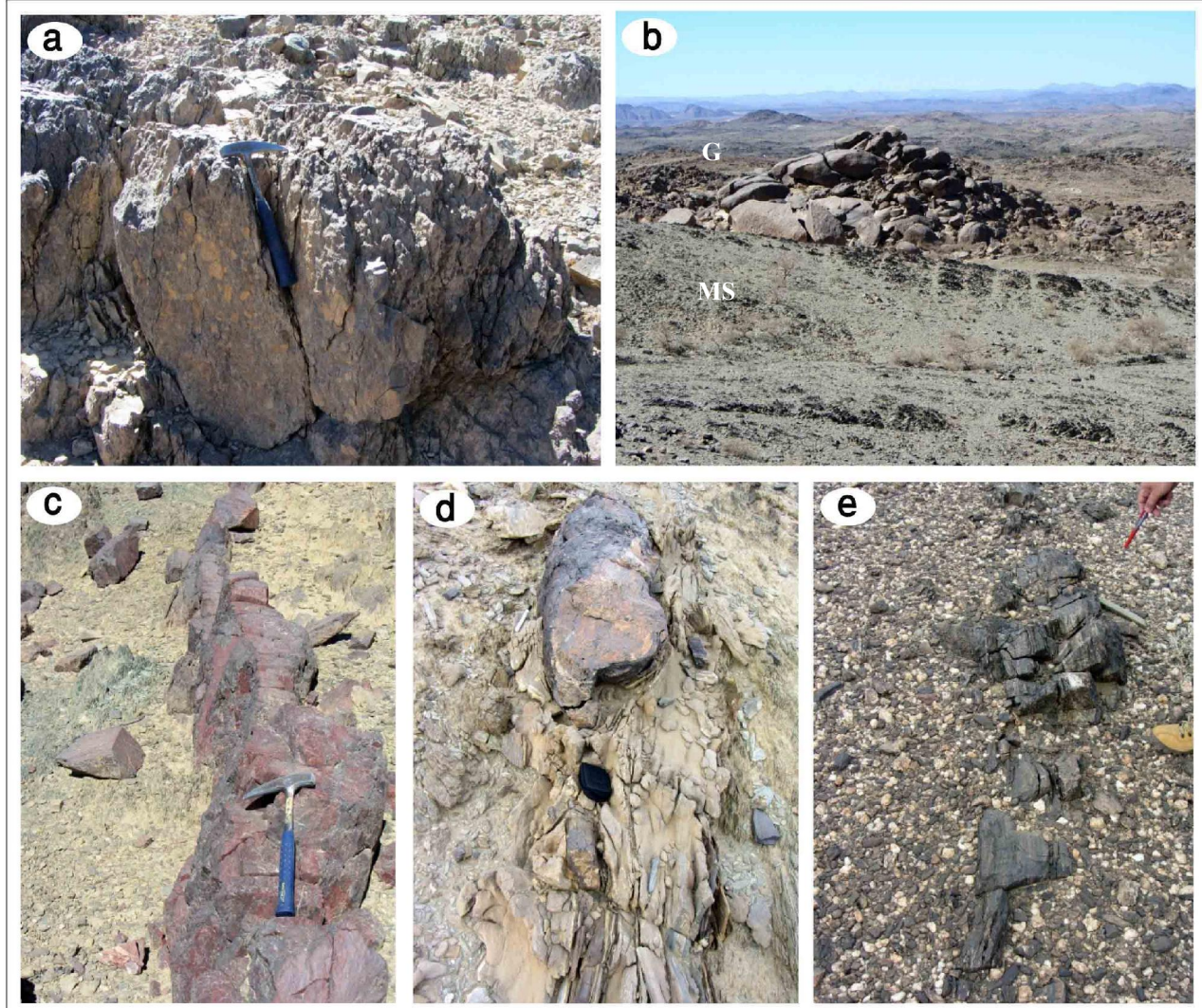


Figure 18. Field photographs showing the mineralizing-related criteria: (a) Hydrothermal breccia that are approximately 8 km north of the Al-Hajar mine, (b) the porphyritic dike-like body of granite “G” that intrudes the metasediments, “MS” considered as the source of the hydrothermal activities in the area, (c) subvertical jasper parallel to the foliation in the metasediments (d) thick boudinaged mineralized quartz vein in the metasediment of the target area, and (e) a mineralized quartz vein in the prospect area.

4. Geometrical analysis

Foliations, lineations and fold hinges of small folds were measured during this study. They are presented on the maps in Figs. 14 & 15. The measured attitudes of 78 foliation planes throughout the mapped areas are projected on an equal-area stereonet using the OpenStereo program. Inspection of the diagram (Fig. 20a) shows that the foliation mainly strike SSE and steeply SW dipping. Few foliation planes are striking in the NNW and moderately dip toward the NE. The variation in the foliation attitudes is due to

refolding. The diagram also shows that the major fold axis is gently plunging due north with the subvertical axial plane. The rose diagram for the strike direction of the 78 measured foliation planes is shown in Fig. 20b; the diagram shows that the main strike direction is due SSE, and few foliations are NNW-striking.

Based on the field relations and the geometrical analysis of the investigated areas, three phases of deformation are recognized. Every single event has its structural elements and its tectonic regime, as summarized in Table 1.

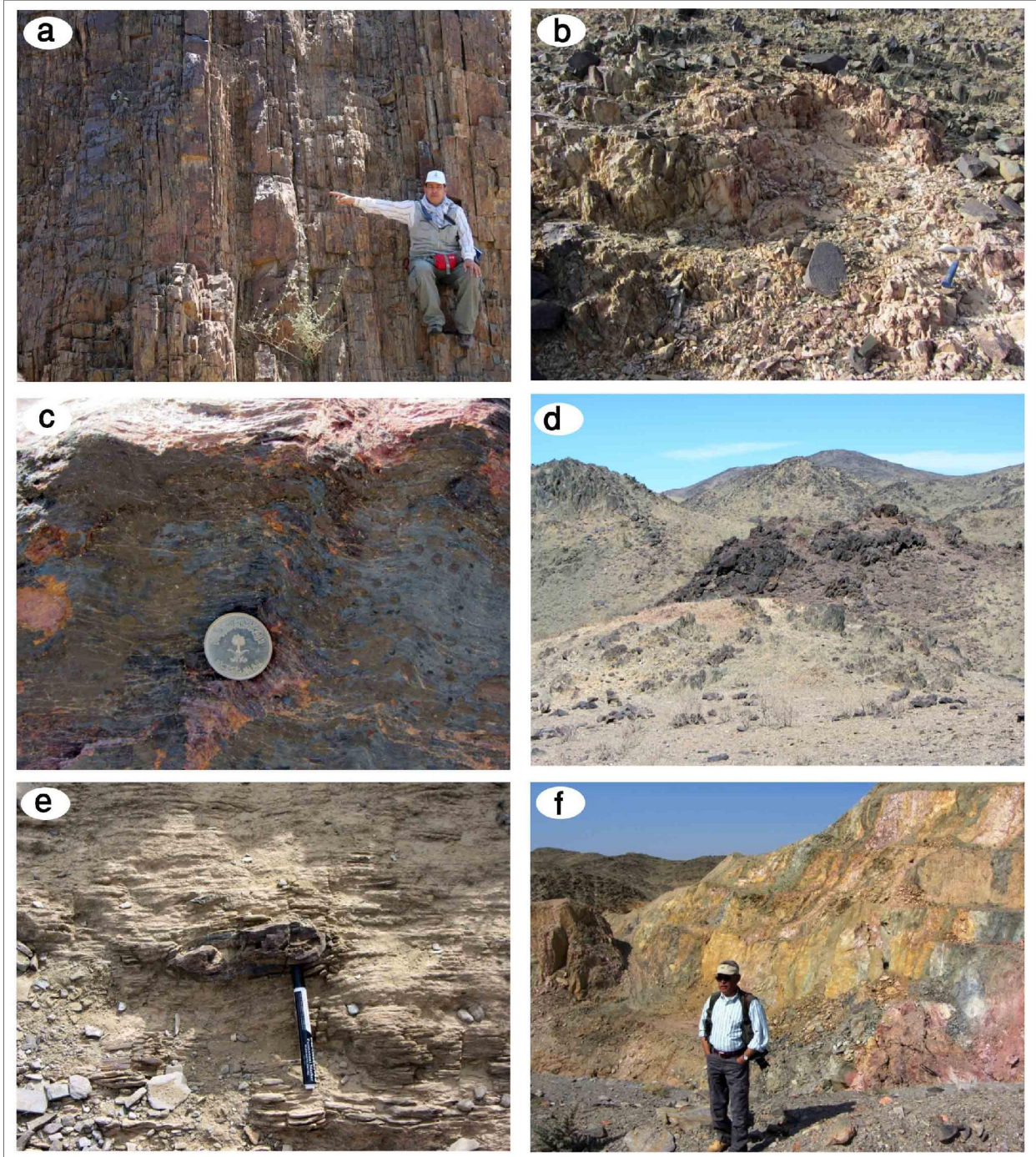


Figure 19. Field photographs showing the rock alteration-related features: (a) subvertical foliation in the metasediments, looking S, (b) alteration zone in the metasediments, (c) folded and oxidized iron gossans related to the massive sulphide ore deposits, (d) mountain size of the iron gossan, “Igs,” in a huge altered zone of the metasediments located approximately 8 km north of the Al-Hajar mine, (e) isolated lenses or boudinaged mineralized quartz parallel to the foliation planes in the metasediments, and (f) an open pit site in the Al-Hajar area in the altered metasediments.

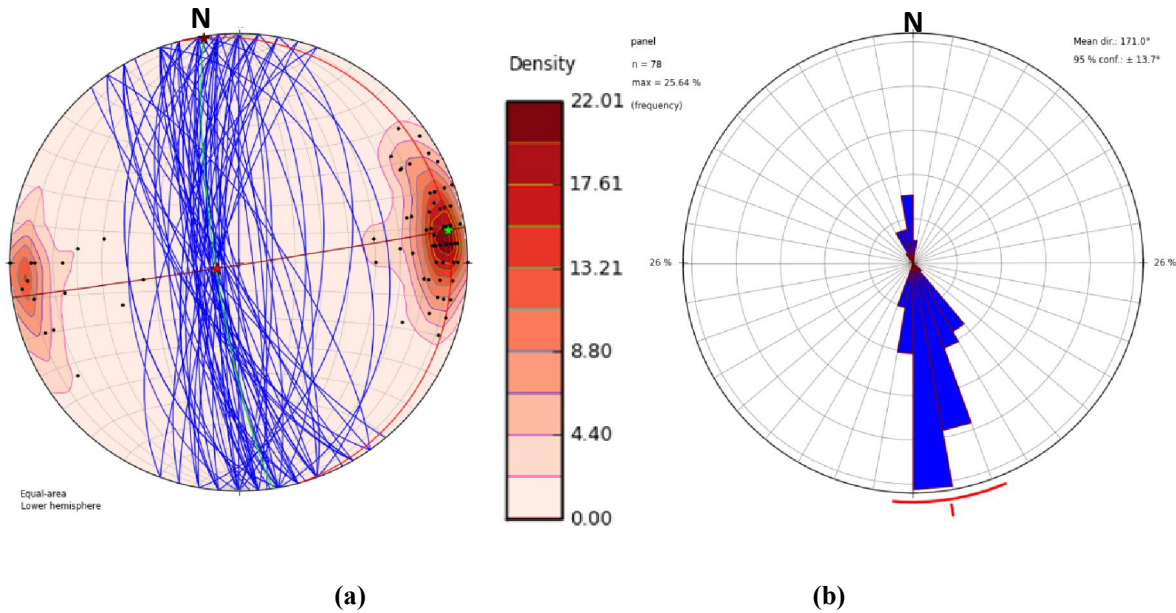


Figure 20. Stereographic projection (a) an equal-area lower hemisphere stereonet of the poles. The great circles and contours of 78 foliation planes were measured throughout the entire mapped area "prospect and target"; inspection of the diagram clearly indicates that the foliations are striking approximately N-S and steeply to moderately dip due SW and NE and (b) a rose diagram showing that the main strike directions are SSE.

Table 1. Results of the field data collected from the prospect and the target areas.

Inspected features	The prospect area: "Hajar site"	The target area: "west Al-Aqiq"
Rock units	Metasediments (slates, phyllites and schists) and metavolcanics, (rhyolite and andesite) were intensively altered.	Metasediments (slates and phyllites) and metavolcanics (andesite) Metavolcanics were locally altered, whereas metasediments were mostly altered.
Metamorphic grade	Low-grade, green-schist facies	Low-grade, green-schist facies
Structural elements	- A series of nearly N-S trending anticline and syncline folds with subvertical axial plane foliations, shear zones (ductile and brittle-ductile). Local thrust-related structures along the contact with igneous intrusions. Three phases (D ₁ -D ₃) of deformation: the first and the second phases are compressional, and the third phase is a transpressional regime.	- A series of nearly N-S trending anticline and syncline folds with subvertical axial plane foliations, ductile shear zones with dextral sense of shear "top-to-the-north." - Three phases (D ₁ -D ₃) of deformation: the first and the second phases are compressional, and the third phase is a transpressional regime.
Plutonic intrusions	- Diorite and porphyritic granite	- Diorite and grey granite
Mineral signs	- Hydrothermal breccia, -iron gossans and Jasper, -alteration zones	- Mineralized quartz vein system, - alteration zones
Deposit type	- Porphyry-type deposits	- Hydrothermal vein-type deposits

5. Conclusions

The lithological units and the structural element framework of the study area were mapped in detail during this study on a scale of 1:20,000. A detailed analysis of the processed Landsat ETM+ and SPOT-5 imagery was performed by mapping the studied areas.

The color signatures of some rock units are easily recognized and visually interpreted on the Landsat ETM+ and SPOT-5 images. The rock units primarily include porphyry granite, diorites, metasediments and metavolcanics. This study revealed the following conclusions:

- The Al-Hajar area is located in Asir terrane in the south central part of the Arabian Shield. It is covered by Precambrian metasediments and metavolcanics of low-grade green-schist facies rocks. They are intruded by many igneous plutonic bodies.

- Different image processing techniques, such as image enhancement and image ratios, are applied in this work for the lithological and structural discrimination of the investigated area.

- The processed Landsat color composite image and the Landsat ratio image assisted in providing more lithological and structural information for the study area. The detailed geological map of the investigated area on a scale of 1:20,000 was constructed using the SPOT-5 constructed images. The constructed new geological map of the study area was verified in the field. It is recommended to apply the different image processing techniques with high spectral and spatially resolved satellite digital data for detailed geological mapping.

- The host rocks of the mineralization are green-schist facies with metasedimentary and metavolcanic rocks of Pre-Cambrian age.

- Three phases of successive deformation were determined during this study (D_1 - D_3): The first and the second phases are compressional, while the third phase is a transpressional regime. A series of nearly N-S trending anticline and syncline folds of tight to isoclinal type are associated with D_1 . Subvertical axial plane foliations, deformed pebbles, rod and pencil structures were recorded. Dextral shear zones "top-to-north" of either ductile or brittle-ductile nature were also detected and developed during D_3 .

- The field data and geometrical analysis indicate the presence of at least two fold generations (F_1 and F_2). F_1 -folds are a series of isoclinal anticline and syncline folds of gently plunging axis due north, whereas F_2 trends N 10° E and dips 65 degrees.

- The local thrust-related structures are determined along the contact with igneous intrusions.

- Mineralization is generally associated with N-S ductile shearing in which most of the hydrothermal alteration zones are presented.

- The alteration zone, hydrothermal breccia, Iron gossans and Jasper either dike-like body or thick veins are among the mineral indicators that were recognized and analyzed during this study.

- There is field evidence to support the possibility of Porphyry-type and hydrothermal vein-type deposits in the Al-Hajar mine area and the target area "west of Al-Aqiq", respectively.

- The spectral signature of the Al-Hajar gold mining prospect was used in this study as a guide to locate new similar sites, which are considered to be target areas. The results of the current study are applicable for detecting target areas in any other altered low-grade metamorphic belts.

Acknowledgments

This work was funded by the Deanship of Scientific Research (DSR), King Abdulaziz University, Jeddah, under grant No. (49/145/1434). The authors, therefore, acknowledge with thanks DSR technical and financial support. We would also like to show our gratitude to A. Hassan and A. Abdel-Latief our colleagues from Faculty of Earth Sciences, King Abdulaziz University for fruitful discussion.

Correspondence to:

Mohamed K. El-Shafei
Faculty of Earth Sciences, Building 55, King Abdulaziz University, Jeddah, P.O. Box: 80206 Jeddah: 21589, Saudi Arabia
Telephone: +966540322415
Emails: mshafei@kau.edu.sa or elshafeim@yahoo.com

References

1. Abrams MJ, Brown D, Lepley L, Sadowski R. Remote sensing for porphyry copper deposits in southern Arizona. *Economic Geology* 1983; 185 (78): 591-604.
2. Al-Shanti AMA. *Geology of the Arabian Shield of Saudi Arabia*. Scientific Publishing Centre, King Abdulaziz University, 2009; 1st ed., 190p. Jeddah.
3. Amer R, Kusky T, Ghulam A. Lithological mapping in the Central Eastern Desert of Egypt using ASTER data. *Journal of African Earth Sciences* 2009; 56 (2):75-82. DOI: 10.1016/j.jafrearsci.2009.06.004.
4. Antonielli B, Fidolini F, Righini G. Landsat TM and Quickbird images for geological mapping in the syn-rift Lower Dogali Formation (Red Sea coast, NE Eritrea). *PHOTO INTERPRETATION* 2009; 3: 107-114.
5. Bamoussa AO. Infracambrian superimposed tectonics in the Late Proterozoic units of Mount

- Ablah area, southern Asir terrane, Arabain Sheild, Saudi Arabia. Arab Journal of Geosciences 2013; 6: 2035-2044.
6. Bernstein R. Digital image processing for remote sensing, IEEE press 1978.
 7. Bishta AZ. Lithologic discrimination of Gabal Qattar-Um Disi environs, North Eastern Desert of Egypt using thematic mapper data of Landsat-7. The third International Symposium on Geophysics, Tanta University, Tanta, Egypt, 2004; 541-557.
 8. Bishta A Z. Lithologic discrimination using selective image processing techniques of Landsat-7 data, Um Bogma environs, West central Sinai, Egypt. Journal of King Abdulaziz University (JKAU): Earth Sciences 2008; 21:193-213.
 9. Bishta A Z. Assessing utilization of multi-resolution Satellite imageries in geological mapping, a case study of Jabal Bani Malik area, eastern Jeddah city, Kingdom of Saudi Arabia. Journal of King Abdulaziz University (JKAU): Earth Sci. 2010; 21 (1) 27-52.
 10. Blenkinsop TG, Doyle, MG. Structural controls on gold mineralization on the margin of the Yilgarn craton, Albany-Fraser orogen: The Tropicana deposit, Western Australia. Journal of Structural Geology 2014; 67: 189-204.
 11. Cox SF. Deformational Controls on the Dynamics of Fluid Flow in Mesothermal Gold Systems. In: Geological Society, London 1999; Special Publications 155: 123-140.
 12. Davis PA, Berlin GL. Rock discrimination in the complex geological environment of Jabal Salma, Saudi Arabia using Landsat Thematic Mapper data. Photogrammetric Engineering & Remote Sensing 1989; 7: 1147-1160.
 13. Deksissa DJ, Koeberl C. Geochemistry, alteration, and genesis of gold mineralization in the Okote area, southern Ethiopia. Geochemical Journal 2004; 38:307-331.
 14. Doyle MG, Fletcher IR, Foster J, Large RR, Mathur R, McNaughton NJ, Meffre S, Muhling JR, Phillips D, Rasmussen B. Geochronological Constraints on the Tropicana Gold Deposit and Albany-Fraser Orogen, Western Australia. Economic Geology 2013; 110: 355-386.
 15. El Janati M, Soulaïmani A, Admou H, Youbi N, Hafid A, Hefferan KP. Application of ASTER remote sensing data to geological mapping of basement domains in arid regions: a case study from the Central Anti-Atlas, Iguerda inlier, Morocco. Arabian Journal of Geosciences 2013; 7 (6): 2407-2422.
 16. El-Shafei MK. Structural control on Banded iron Formation (BIF) and Gold mineralization at Abu Marawat area, Central Eastern Desert, Egypt. Journal of King Abdulaziz University (JKAU): Earth Sciences 2011; 22 (2): 155-183.
 17. Gibson J, Power CH. Introductory remote sensing digital image processing and application. London: Routledge 2000.
 18. Guha A, Kumar KV, Rao EN, Parveen R. An image processing approach for converging ASTER-derived spectral maps for mapping Kolhan limestone, Jharkhand, India. Current Science 2014; 106 (1): 40-49.
 19. Gupta RP. Remote sensing geology. Springer, Berlin 2003, 2nd ed. , 656 p.
 20. Gustafson LB, Quiroga G. Patterns of mineralization and alteration below the porphyry copper orebody at El Salvador, Chile. In: Economic Geology (New Haven) 1995; 90: 2 – 16.
 21. Haselwimmer CE, Riley TR, Liu JG. Assessing the potential of multispectral remote sensing for lithological mapping on the Antarctic Peninsula: case study from eastern Adelaide Island, Graham Land. Antarctic Science 2010; 22 (3): 299–318.
 22. Jutz SL, and Chorowicz J. Geological mapping and detection of oblique extension structures in the Kenyan Rift Valley with a SPOT/Landsat-TM datamerge. International Journal of Remote Sensing 1993; 14: 1677-1688.
 23. Kavak KS, Cetin H. A Detailed Geologic Lineament Analysis Using Landsat TM Data of Golmarmara/Manisa Region, Turkey. Online Journal of Earth Sciences 2007; 1: 145-153. doi:ojesci.2007.145.153.
 24. Kolb J, Hellmann A, and Rogers A. The Role of a Transcrustal Shear Zone in Orogenic Gold Mineralization at the Ajjanahalli Mine, Dharwar Craton, South India. Economic Geology 2004; 99 (4): 743-759. doi:10.2113/gsecongeo.99.4.743.
 25. Lechi G. Satellite sensors and satellite image characteristic. Rep 11th international training course on applications of remote sensing to agricultural statistics (5-20 May 1986), Remote and Montpellier FAO, Rome 1988.
 26. Lillesand TM, Kiefer RW, Chipman JW. Remote sensing and image interpretation 2004; 4th ed., John Wiley and Sons Inc. New York, ISBN: 0-471-25515-7, 763 p.
 27. Madani A, Bishta AZ. Selection of the optimum bands of Landsat 7 ETM+ for automatic lineaments extraction: A case study of Gattar Granites, North Eastern Desert, Egypt. Geology of the Arab World, Cairo University 2002; 6: 323-360.

28. Mather PM. Computer processing of remotely sensed images, an introduction 1987; John Wiley and Sons, ISBN: 0 – 471 – 9064 –4.
29. PCI Geomatica. Software helps 2003; 9.1.
30. Richards JA. Remote sensing, digital image processing, an introduction 1995; Springer-Verlag New York, Inc. Secaucus, NJ, USA. ISBN: 0387548408.
31. Sabins FF. Remote sensing for mineral exploration. *Ore Geology Reviews* 1999; 14: 157–183.
32. Schowengerdt RA. Techniques for image processing and classification in remote sensing. Academic Press, Inc., US, 1983; ISBN: 0 – 12-62890 – 8.
33. Sultan M, Arvidson RE, Sturchio NC. Mapping of serpentinites in the Eastern Desert of Egypt by using Landsat Thematic Mapper data. *Geology* 1986; 14: 995-999. Available at: <http://glovis.usgs.gov>.
34. Sultan M, Arvidson RE, Sturchio NC, Guinness EA. Lithologic mapping in arid regions with Landsat thematic mapper data: Meatiq dome, Egypt. *Geological Society of America Bulletin* 1987; 99: 748-762.
35. Wielen VS, Oliver S, Kalinowski A. Remote sensing and spectral investigations in the western succession, mount Isa Inlier, implications for exploration. Predictive mineral discovery CRC Conference 2004, Barossa Valley 1-3 June 2004.
36. Williams-Jones AE, Heinrich CA. Vapor transport of metals and the formation of magmatic-hydrothermal ore deposits. In: *Econ. Geol.* (New Haven) 2005; 100: 1287 – 1312.

9/4/2015